Journal of Sound and Vibration 329 (2010) 644–658

Contents lists available at ScienceDirect

Journal of Sound and Vibration

journal homepage: www.elsevier.com/locate/jsvi

Accurate identification of the frequency response functions for the rotor–bearing–foundation system using the modified pseudo mode shape method

Yeong-Shu Chen [a,*], Ye-Dar Cheng [a], Tachung Yang [a], Kwang-Lu Koai [b]

[a] Department of Mechanical Engineering, Yuan-Ze University, Chungli 320, Taiwan, ROC
[b] Taiwan Power Research Institute, Taipei 100, Taiwan, ROC

ARTICLE INFO

Article history:
Received 26 August 2008
Received in revised form
26 September 2009
Accepted 27 September 2009
Handling Editor: L.G. Tham
Available online 7 November 2009

ABSTRACT

In this paper, an identification technique in the dynamic analyses of rotor–bearing–foundation systems called the *pseudo mode shape method* (PMSM) was improved in order to enhance the accuracy of the identified dynamic characteristic matrices of its foundation models. Two procedures, namely, phase modification and numerical optimisation, were proposed in the algorithm of PMSM to effectively improve its accuracy. Generally, it is always necessary to build the whole foundation model in studying the dynamics of a rotor system through the finite element analysis method. This is either unfeasible or impractical when the foundation is too complicated. Instead, the PMSM uses the frequency response function (FRF) data of joint positions between the rotor and the foundation to establish the equivalent mass, damping, and stiffness matrices of the foundation without having to build the physical model. However, the accuracy of the obtained system's FRF is still unsatisfactory, especially at those higher modes. In order to demonstrate the effectiveness of the presented methods, a solid foundation was solved for its FRF by using both the original and modified PMSM, as well as the finite element (ANSYS) model for comparisons. The results showed that the accuracy of the obtained FRF was improved remarkably with the modified PMSM based on the results of the ANSYS. In addition, an induction motor resembling a rotor–bearing–foundation system, with its housing treated as the foundation, was taken as an example to verify the algorithm experimentally. The FRF curves at the bearing supports of the rotor (armature) were obtained through modal testing to estimate the above-mentioned equivalent matrices of the housing. The FRF of the housing, which was calculated from the equivalent matrices with the modified PMSM, showed satisfactory consistency with that from the modal testing.

© 2009 Elsevier Ltd. All rights reserved.

1. Introduction

In the construction of the typical industrial machinery, the rotor, bearings, and foundation are often perceived as the main components of rotating machinery systems. Among these types of machines, the turbomachinery used in power plants is much larger than the smaller ones, such as the lathe or milling machines commonly used in machine shops. To ensure the system's stability under designed working speeds, the foundations of machine structures tend to be more

* Corresponding author. Tel.: +886 3 4638800x2473; fax: +886 3 4517113.
E-mail address: yschen@saturn.yzu.edu.tw (Y.-S. Chen).

0022-460X/$ - see front matter © 2009 Elsevier Ltd. All rights reserved.
doi:10.1016/j.jsv.2009.09.038

complicated and stronger than ever for those low-speed machines, such as the former, and for the high-speed cutting machines like the latter. The foundation effects then become more significant in determining the dynamic properties of the system. Kang et al. [1] discussed the effects of simplistic foundations as the lumped-mass, continuous-beam, and plate-type forms on the dynamic characteristics of the rotor systems. A stiffer foundation suspension along with the larger foundation size was suggested to enlarge the range of operating speed and to avoid the rigid-body motion of the foundation within a given range of the operating speed.

Nevertheless, design analysts often find that even with the use of a sophisticated computer software program, it is still difficult and time-consuming to establish complex system models using the finite element (FE) method. Many researchers have attempted to establish the accurate foundation models from the experimental data without using the FE method. To date, foundation identification methods can generally be classified into two categories: (a) methods based on the data from the frequency response function (FRF) curves that are adopted from the experimental modal testing of the foundation alone (excluding the rotor) [2–8], and (b) methods using vibration data at the rotor or the foundation in the run-down or run-up of whole systems [9–16].

For the former methods, the modal parameters, modal matrix, and equivalent matrices of the most significant modes are estimated from the FRF data of the foundation and are introduced into the equation of motion for the overall system in order to explain the foundation behaviour. Conversely, the second type of identification method does not require researchers to perform the modal testing. Instead, these methods use the transient vibration data at the rotor journals or bearing supports to establish the foundation models. In recent years, these methods have been adopted to identify, locate, and evaluate the severity of the rotating machinery's malfunction [17–19].

Using run-up or run-down data to identify the foundation characteristics is perhaps more suitable and convenient than using FRF data in practice. The methods with run-up or run-down data require knowing more correct system information such as rotor models and bearing characteristics. The actual challenge is to find the methods that can withstand noise and modelling errors. When systems have the design characteristic of easy rotor disassembly, the methods using the FRF data of foundations are usually well considered. The major disadvantage of using FRF data is that the number of modes identified must equal the number of measured degrees of freedom (DOFs). If more accurate dynamic properties of the system are to be obtained, more measuring points should be added to the substructure.

As a result, an innovative strategy called the *pseudo mode shape method* (PMSM) was presented by Yang et al. [20,21]. This method adopted the FRF data at the joint points between the mother structure and the substructure in order to identify the equivalent matrices with complex numbers for the 2-D beam and 3-D bearing support substructures. The PMSM has the advantageous feature of not requiring the number of modes identified to be equal to the number of measured DOFs in the modelling of the substructure.

The aim of this paper is to substantially improve the accuracy of PMSM by introducing the procedures of phase modification and numerical optimisation. The procedures determined the foundation's equivalent mass, damping, and stiffness matrices with real numbers instead of complex numbers through the phase modification technique. It can readily be integrated into the FE model of the commercial software or self-developed programs for replacing the foundation's model. Thus, a significantly large amount of modelling efforts and computing time are saved. However, some of the commercial FE software either do not have the ability to allow users to access the data files to change the matrices, or alter limitations on the matrices' size. Therefore, the identified equivalent matrices were used in the authors' self-developed FE software [22] to replace the foundation model in solving the system's FRFs.

For verification purposes, the typical FE analysis of a full rotor-bearing-foundation system model was constructed with the commercial ANSYS 10.0 software to obtain the FRF of the full system. In the meantime, the model of foundation alone (excluding all others, such as bearing and rotor) was also excited with a harmonic force at bearing joint positions to obtain the FRF of these positions. The foundation's FRF at the contact points of the rotor was then identified in the modified PMSM to solve for the identified equivalent mass, damping, and stiffness matrices. Finally, the solid foundation in this case was removed and replaced with the equivalent mass, damping, and stiffness matrices in the FE model of the authors' analysis program to solve for the full system's FRF. As calculated with the current algorithm, the resulting FRFs of the system were found to be extremely close to those of the ANSYS's. In addition, these identified equivalent matrices can be used to solve back for the foundation's FRF to check its correctness when compared to that of the ANSYS's. All the results showed that a highly accurate dynamic analysis could be achieved with the proposed method. Other than the above-mentioned numerical verification, an experimental modal testing on a realistic motor housing was also conducted to obtain the above-mentioned equivalent matrices of its dynamic characteristics. The FRF of the realistic motor housing was also compared with that from the modified PMSM in order to show its practical applications in various engineering problems.

2. Fundamentals of the modified pseudo mode shape method

With the procedures of phase modification and numerical optimisation introduced into the PMSM, the suitable components of the respective mode shape vectors (denote each individual mode) in representing the foundation were thus determined. Hereafter, the pseudo mode shape matrix was built through the column arrangement of these mode shape vectors. With the pseudo mode shape matrix and modal parameters, the equivalent mass, damping, and stiffness matrices

of the foundation were then estimated. These equivalent matrices, combined with the FE rotor model and bearing coefficients, became the equation of motion for the whole system.

2.1. Definition of frequency response functions

The derivative processes of FRFs are described here, and the details can be found in [23]. The FRF data of any structure can also be obtained through experimental modal testing or by means of the FE simulation method. For the vibration equation of a system, the mathematical model can be expressed as follows:

$$[M]\{\ddot{x}\} + [C]\{\dot{x}\} + [K]\{x\} = \{f\}, \tag{1}$$

where $[M]$, $[C]$, and $[K]$ are the mass, damping, and stiffness matrices of the system, respectively. Moreover, $\{x\}$ and $\{f\}$ are the displacement and external force vectors, respectively. In Eq. (1), the displacement vector of the system can be represented in the modal coordinate with the following mode shape matrix:

$$\{x\}_{N\times 1} = \sum_{r=1}^{N} \eta_r \{V_r\} = [U]_{N\times N}\{\eta\}_{N\times 1} \tag{2}$$

where N is the total number of components in the modal coordinate; η_r and $\{V_r\}$ are the components of the modal coordinate and the mode shape vector at the rth mode, respectively; $[U]=[\{V_1\},\{V_2\}, \ldots, \{V_N\}]$ denotes the mode shape matrix; and $\{\eta\}=\{\eta_1,\eta_2, \ldots, \eta_N\}^T$ refers to the modal coordinate vector. Substituting Eq. (2) into Eq. (1), the equation of spatial motion is transformed into the equation of decoupled motion:

$$[M][U]\{\ddot{\eta}\} + [C][U]\{\dot{\eta}\} + [K][K]\{\eta\} = \{f\}. \tag{3}$$

Multiplying the matrix $[U]^T$ at both sides of Eq. (3) produces the following:

$$\left[\not{m}\right]\{\ddot{\eta}\} + \left[\not{c}\right]\{\dot{\eta}\} + \left[\not{k}\right]\{\eta\} = [U]^T\{F\} = \{\mu\}, \tag{4}$$

where $\left[\not{m}\right]$, $\left[\not{c}\right]$, and $\left[\not{k}\right]$ are the diagonal mass, damping, and stiffness matrices, respectively; and $\{\mu\}$ is the modal force vector.

The equation of motion at the rth mode is represented as follows:

$$m_r\ddot{\eta}_r + c_r\dot{\eta}_r + k_r\eta_r = \mu_r, \tag{5}$$

where $\mu_r = \{V_r\}^T\{f\} = \sum_{j=1}^{N} \phi_{jr} f_j$ and ϕ_{jr} are the jth components of the rth mode shape vector. By considering the harmonic excitation acting on the system, the component of the modal coordinate and the modal force at the rth mode can be designated as $\eta_r = \hat{\eta}_r e^{i\omega t}$ and $\mu_r = \hat{\mu}_r e^{i\omega t}$, respectively. Eq. (2) becomes the summation of a series consisting of the exciting force, components of the mode shape, and the modal parameters:

$$\{\hat{x}\}_{N\times 1} = \sum_{r=1}^{N} \hat{\eta}_r\{V_r\} = \sum_{r=1}^{N}\sum_{j=1}^{N} \frac{\phi_{jr}\hat{f}_j}{m_r[\omega_r^2 - \omega^2 + 2i\omega\xi_r\omega_r]}\{V_r\}, \tag{6}$$

where $\{x\} = \{\hat{x}\}e^{i\omega t}$ is the displacement vector of the spatial model, and $f_j = \hat{f}_j e^{i\omega t}$ is the exciting force. In addition, ω_r and ξ_r stand for the rth natural frequency and damping ratio (called modal parameters), respectively. Considering just a single component $\hat{f}_j$ of the exciting force, the ith component of the displacement vector can be rewritten as

$$\hat{x}_i = \sum_{r=1}^{N}\sum_{j=1}^{N} \frac{\phi_{ir}\phi_{jr}\hat{f}_j}{m_r[\omega_r^2 - \omega^2 + 2i\omega\xi_r\omega_r]}. \tag{7}$$

The FRF H_{ij} is defined as the ratio of the ith displacement component $\hat{x}_i$ to the jth exciting force component $\hat{f}_j$. It can also be shown as follows:

$$\frac{\hat{x}_i}{\hat{f}_j} = H_{ij} = \sum_{r=1}^{N} H_{ij,r} = \sum_{r=1}^{N} \frac{\phi_{ir}\phi_{jr}}{m_r[\omega_r^2 - \omega^2 + 2i\omega\xi_r\omega_r]} \tag{8}$$

where $H_{ij,r}$ is the peak value of FRF at the rth mode. Eq. (8) represents the relationship between the single exciting force and displacement. However, the situation of multiple excitations is not considered in the following theory.

2.2. The pseudo mode shape method

The simple scheme of a rotor–bearing–foundation system shown in Fig. 1 demonstrates the PMSM operation. The rotor was treated as the mother structure, while the foundation and two bearing supports were treated as the substructure. Considering only the translation DOFs in the X and Y directions at each of the bearing supports, the mode shape vectors of the bearing–foundation structure were represented with a total of four DOFs. Eq. (8) involves the first four natural

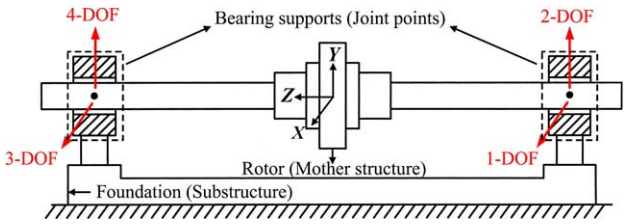

Fig. 1. Schematic of a rotor–bearing–foundation system.

frequencies (N=4) that can be expressed as follows:

$$H_{ij} = \frac{\phi_{i1}\phi_{j1}}{m_1[\omega_1^2 - \omega^2 + 2i\omega\xi_1\omega_1]} + \frac{\phi_{i2}\phi_{j2}}{m_2[\omega_2^2 - \omega^2 + 2i\omega\xi_2\omega_2]} + \frac{\phi_{i3}\phi_{j3}}{m_3[\omega_3^2 - \omega^2 + 2i\omega\xi_3\omega_3]} + \frac{\phi_{i4}\phi_{j4}}{m_4[\omega_4^2 - \omega^2 + 2i\omega\xi_4\omega_4]}, \tag{9}$$

where i=1,2,, …, 4 and j=1,2, …, 4. Assume that the first term at the right-hand side of Eq. (9) was dominant in affecting the values of the FRFs when $\omega=\omega_1$, whereas the other terms had a weak influence on these FRFs. Thus, the second, third, and fourth terms can be omitted. The simplified form of Eq. (9) can now be presented as follows:

$$H_{ij,1} = \frac{\phi_{i1}\phi_{j1}}{m_1 2i\xi_1\omega_1^2}. \tag{10}$$

As mentioned, with two DOFs at each of two bearing supports, there were a total of four DOFs for all of the supports of the whole system. After this, a 4×4 symmetric frequency response function matrix was built as follows:

$$\text{FRF matrix} = \begin{bmatrix} H_{11,r} & & & \\ H_{21,r} & H_{22,r} & & \\ H_{31,r} & H_{32,r} & H_{33,r} & \\ H_{41,r} & H_{42,r} & H_{43,r} & H_{44,r} \end{bmatrix}. \tag{11}$$

At the first mode ($r = 1$), the available peak values in the FRF data were denoted as $H_{11,1}$, $H_{21,1}$, $H_{31,1}$, $H_{41,1}$, $H_{22,1}$, $H_{32,1}$, $H_{42,1}$, $H_{33,1}$, $H_{43,1}$, and $H_{44,1}$. These values can then be utilised to evaluate the related components. The chosen four items of the values $H_{11,1}$, $H_{21,1}$, $H_{31,1}$, and $H_{41,1}$ with $\omega=\omega_1$, $\xi=\xi_1$, and m_1=1 were used to evaluate the components $\phi_{11}=\phi_{41}$ of the first pseudo mode shape vector. The procedures are indicated as follows:

$$\phi_{11} = \sqrt{2i\xi_1\omega_1^2 H_{11,1}}, \tag{12a}$$

$$\phi_{21} = 2i\xi_1\omega_1^2 H_{21,1}/\phi_{11}, \tag{12b}$$

$$\phi_{31} = 2i\xi_1\omega_1^2 H_{31,1}/\phi_{11}, \tag{12c}$$

$$\phi_{41} = 2i\xi_1\omega_1^2 H_{41,1}/\phi_{11}. \tag{12d}$$

The components of the other pseudo mode shape vectors ϕ_{1r}–ϕ_{4r} (r=2,3,4) at the second, third, and fourth natural frequencies can also be estimated in this manner. The pseudo mode shape matrix [U] was constructed using four mode shape vectors{V_r} (r=1, 2, …, 4) with the components ϕ_{1r}–ϕ_{4r} in each vector:

$$[U] = [V_1, V_2, V_3, V_4] = \begin{bmatrix} \phi_{11} & \phi_{12} & \phi_{13} & \phi_{14} \\ \phi_{21} & \phi_{22} & \phi_{23} & \phi_{24} \\ \phi_{31} & \phi_{32} & \phi_{33} & \phi_{34} \\ \phi_{41} & \phi_{42} & \phi_{43} & \phi_{44} \end{bmatrix}. \tag{13}$$

Finally, the equivalent mass, damping, and stiffness matrices were established as follows:

$$[M^E] = ([U]^T)^{-1}[\quad][U]^{-1}, \tag{14a}$$

$$[C^E] = ([U]^T)^{-1}[\quad][U]^{-1}, \tag{14b}$$

$$[K^E] = ([U]^T)^{-1}[\quad][U]^{-1}. \tag{14c}$$

2.3. Phase modification

The actual peak values of the FRF curves are often inaccurate owing to the limited resolution of the data. This causes deviation in the FRF curves of the original substructure and those of the equivalent substructure. Nevertheless, the defect can be improved with phase modification at the resonance peaks. The peak values of the FRFs can be expressed as the following complex numbers:

$$H_{ij,r} = |H_{ij,r}|\cos\theta + i|H_{ij,r}|\sin\theta. \tag{15}$$

When at the resonance peaks of a single degree of freedom system, the analytic phase difference between the excitation and the response is either θ=+90° or θ=−90°. The criteria of phase modification at the resonance peaks were defined as follows:

(a) If

$$\tan^{-1}\left(\frac{\text{imaginary part of } H_{ij,r}}{\text{real part of } H_{ij,r}}\right) \approx +90^{\circ}, \quad H_{ij,r} = +|H_{ij,r}|i, \tag{16a}$$

(b) If

$$\tan^{-1}\left(\frac{\text{imaginary part of } H_{ij,r}}{\text{real part of } H_{ij,r}}\right) \approx -90^{\circ}, \quad H_{ij,r} = +|H_{ij,r}|i, \tag{16b}$$

Substituting Eqs. (16a) and (16b) into Eqs. (12a)–(12d), the mode shape vectors ϕ_{1r}, ϕ_{2r}, ϕ_{3r} and ϕ_{4r}, and the pseudo mode shape matrix were obtained.

2.4. Numerical optimisation

If the number of the components of the mode shape vectors ϕ_{1r}–ϕ_{4r} equals the number of the chosen peak values $H_{11,1}$, $H_{21,1}$, $H_{31,1}$ and $H_{41,1}$, the pseudo mode shape vectors can be directly estimated by referring to the procedures detailed in Eqs. (12a)–(12d). However, some other peaks such as $H_{22,r}$, $H_{32,r}$, $H_{42,r}$, $H_{33,r}$, $H_{43,r}$, and $H_{44,r}$ were not considered. To accurately evaluate the components of the pseudo mode shape vectors, it became necessary to use all the peak values.

Here, the procedure of numerical optimisation was introduced to search for the optimum components of the pseudo mode shape vectors with consideration of all the peak values. Referring to Eq. (10), a peak value $H_{ij,r}$ was defined as the observed value in the FRF curve, and a predicted value was defined as $\phi_{ir}\phi_{jr}/m_r 2i\xi_r\omega_r^2$. Given the set of components ϕ_{ir} and ϕ_{jr}, the normalised residual function $\overline{R}(\phi_{ir}, \phi_{jr})$ representing the deviation between the observed value and the predicted one was expressed as follows:

$$\overline{R}(\phi_{ir}, \phi_{jr}) = \frac{\phi_{ir}\phi_{jr}}{H_{ij,r} m_r 2i\xi_r\omega_r^2} - 1. \tag{17}$$

To make the obtained peak value from the mathematical model of prediction $\phi_{ir}\phi_{jr}/m_r 2i\xi_r\omega_r^2$ closer to the observed peak value $H_{ij,r}$, the residual value should be as small as possible.

Therefore, with the intention to drive M predicted values closer to the corresponding peak values, the sum of the square of all normalised residual values at the rth mode must be minimised. As such, an optimisation model for minimising the objective function $F(\phi_{ir}, \phi_{jr})$, which was defined as the sum of square of the normalised residual functions with the set of variables ϕ_{ir} and ϕ_{jr}, was expressed as follows:

$$\text{Minimise}: \ F(\phi_{ir}, \phi_{jr}) = \sum_{m=1}^{M} (W_{ij,r}\overline{R}(\phi_{ir}, \phi_{jr})^2)_m, \tag{18a}$$

$$\text{Initial values}: \ \phi_{ir} = \phi_{ir}^*, \phi_{jr} = \phi_{jr}^*, \tag{18b}$$

where $W_{ij,r}$ are the weighting factors represented as real numbers; and ϕ_{ir}^* and ϕ_{jr}^* are the initial values of the variables that can be precalculated from Eqs. (12a)–(12d).

The optimisation problem was solved precisely using the Gauss–Newton method [24], because this can save a substantial amount of computing time and has a great advantage over other methods in many engineering applications. By minimising Eq. (18a), the optimum values of these variables that best match the results from the prediction model to the peak values of FRF curves were thus identified.

2.5. Finite element model of the rotor–bearing–foundaton system

A simple rotor–bearing FE model generally incorporates a rotating shaft that considers the shear effect (the so-called Timoshenko rotor) with two linear bearings that were represented as the bearing coefficients. The rotor and bearing models are described in the literature [25] and have been adopted for study in the field of rotordynamics. The

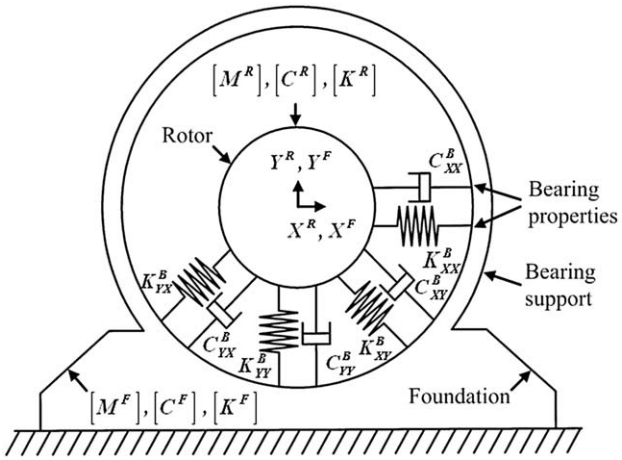

Fig. 2. Mathematical representation of a rotor–bearing–foundation model.

rotor–bearing–foundation model can be presented schematically as shown in Fig. 2, with the superscripts *R*, *B*, and *F* representing the rotor, bearing, and foundation, respectively.

The rotor was located at the centre of the figure as represented by the matrices $[M^R]$, $[C^R]$ and $[K^R]$, and the foundation was denoted as the matrices $[M^F]$, $[C^F]$, and $[K^F]$. The bearings that support the rotor were characterised as the damping matrix $[C^B]$ and the stiffness matrix $[K^B]$. The corresponding elements of these two matrices of the bearing properties are as follows:

$$[C^B] = \begin{bmatrix} C^B_{XX} & C^B_{XY} \\ C^B_{YX} & C^B_{YY} \end{bmatrix}, \tag{19a}$$

$$[K^B] = \begin{bmatrix} K^B_{XX} & K^B_{XY} \\ K^B_{YX} & K^B_{YY} \end{bmatrix}. \tag{19b}$$

The matrices of the rotor structure with the gyroscopic effect were built via the derived rotor element [26]. At the same time, the foundation structure was replaced by the equivalent matrices. By including the equivalent foundation matrices in the rotor–bearing system, it was possible to write the model of the rotor–bearing–foundation system as follows:

$$\begin{bmatrix} M^R & 0 \\ 0 & M^F \end{bmatrix} \begin{Bmatrix} \ddot{Z}^R \\ \ddot{Z}^F \end{Bmatrix} + \begin{bmatrix} C^R + C^B & -C^B \\ -C^B & C^B + C^F \end{bmatrix} \begin{Bmatrix} \dot{Z}^R \\ \dot{Z}^F \end{Bmatrix} + \begin{bmatrix} K^R + K^B & -K^B \\ -K^B & K^B + K^F \end{bmatrix} \begin{Bmatrix} Z^R \\ Z^F \end{Bmatrix} = \begin{Bmatrix} 0 \\ 0 \end{Bmatrix}, \tag{20}$$

where $\{Z\}=\{X,Y\}^T$ is the displacement vector.

Meanwhile, Eq. (20) was used to produce the FRF curves of the rotor–bearing system with the equivalent foundation matrices at the bearing supports. The corresponding results were utilised to examine how close they were to those of the original system constructed with the commercial FE software *ANSYS 10.0*.

3. Rotor–bearing–solid foundation system

The full FE model consisting of a single rotor, two bearing supports, and a solid foundation was built with ANSYS to solve the system's FRF curves. To demonstrate the procedures of the presented algorithm, the foregoing foundation was replaced with the identified mass, damping, and stiffness matrices through both the original PMSM and the modified PMSM methods for comparison. Fig. 3 shows the geometry of the solid foundation, which was constructed out of the cast iron; as can be seen, its bottom area was left hollow. The bearing supports were constructed as a pair of isosceles triangular structures located at both ends of the solid foundation. The whole foundation structure was meshed with three-dimensional elements (series 45 solid element). Each tip of the isosceles triangular structures was set with a lumping mass of 9 kg as the weight of the bearing. Table 1 presents the details of the dimensions of the foundation and the corresponding material properties.

The flexible stiffness K_F of the rotor was defined with the formula F_U/δ, where F_U was the unit force applied at the centre along the length of the rotor while assuming a fixed boundary at both ends of the rotor to produce the defection δ. The grounding stiffness K_{G-Xn} and K_{G-Yn} in the horizontal and vertical directions were set at the four corners (numbered as n=1–4) of the foundation bottom structure. The values of the grounding stiffness were set as $K_{G-X4}=K_{G-Y3}=0.01\times K_F$, $K_{G-X2}=K_{G-X3}=K_{G-Y4}=0.05\times K_F$, $K_{G-Y2}=0.1\times K_F$, and $K_{G-X1}=K_{G-XY1}=1\times K_F$.

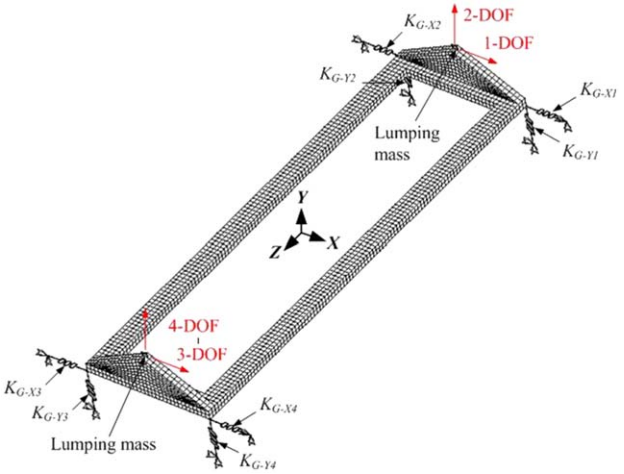

Fig. 3. Schematic of the boundary conditions in a solid foundation.

Table 1
Material properties and dimensions of the solid foundation (thickness: 0.02 m).

Material properties (cast iron)	
Young's modulus ($\times 10^{10}$ Pa)	9.500
Shear modulus ($\times 10^{10}$ Pa)	3.650
Density (kg/m^3)	7250
Poisson's ratio	0.300
Foundation dimensions (bottom hollow board)	
Outer length ($\times 10^{-3}$ m)	1046.610
Outer wide ($\times 10^{-3}$ m)	305.556
Inner length ($\times 10^{-3}$ m)	966.610
Inner wide ($\times 10^{-3}$ m)	225.556
Bearing supports high ($\times 10^{-3}$ m)	76.389

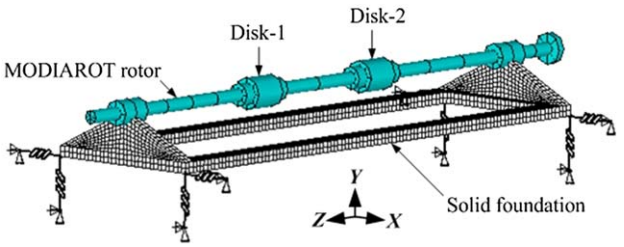

Fig. 4. Finite element model for a rotor–bearing–solid foundation system.

Afterwards, the foundation FRF curves were generated by treating the foundation as the substructure and then taking the output at the two bearing supports using ANSYS. As can be seen in Fig. 1, the DOFs at the two supports in the horizontal direction were represented as 1 and 3, while those in the vertical direction were represented as 2 and 4. Based on the total number of four DOFs at the two joints of the substructure, a total of ten FRF curves were obtained.

The rotor–bearing–solid foundation system is shown in Fig. 4. The rotor model is referred to as the Model based DIAgnostics in ROTating machines (MODIAROT) system as listed in [27]. The rotor has a length of 1.255 m and a weight of 40.110 kg, with a flexible stiffness of K_F=0.305 $\times$ 10^6 N/m. It was modelled with the line element (series 16 pipe element). The bearing coefficients were set to connect the supports of the foundation with the rotor journals. The coefficients were set using mathematical matrices (series 27 matrix element). Each of the 24 rotor nodes had four DOFs with two lateral translations and two bending rotations, and each of the eight nodes at the solid foundation had three DOFs with three lateral translations. There were a total of 10,770 DOFs (2990 elements) in the solid foundation and 10,866 DOFs (3013 elements) in the system.

The full FE model of the rotor–bearing–solid foundation is hereby referred to as the *system with the original solid foundation*. In contrast, the system model for which the equivalent matrices have replaced the foundation in the original

model was referred to as the *system with the equivalent solid foundation*. In this example, the FRF curves of the equivalent whole structure with a static rotor (ignoring the gyroscopic effect) were estimated via the self-developed FE codes [22]. The anisotropic bearings with the stiffness coefficients $K^B_{XX}=1\times10^6$ N/m and $K^B_{YY}=3\times10^6$ N/m were set between the rotor journals and the supports.

4. Identifying the FRF results of the solid foundation system

In this section, the FE model of the solid foundation is hereby referred to as the *original solid foundation,* while the estimated equivalent matrices of the solid foundation are referred to as the *equivalent solid foundation*. These equivalent matrices were further employed to replace the original solid foundation of the whole system to perform the dynamic analysis. This section proved that the differences in the dynamic properties of the original system and those of the system with the equivalent solid foundation can be improved considerably by incorporating the modified procedures into the PMSM.

4.1. Equivalent solid foundation taking the first four sets of modal parameters

The FRF curves of the solid foundation at the supports within the frequency range of 0–50 Hz were previously obtained from the FE model. The resulting FRF curves with the first four sets of modal parameters were used to estimate the pseudo mode shape vectors. In the PMSM, the components of the pseudo mode shape vectors with complex number were obtained via Eqs. (12a)–(12d). Nevertheless, with the phase modification criteria of Eqs. (16a) and (16b) in the modified PMSM, the peak values of the FRF curves can be transformed into pure imaginary numbers. These numbers can be substituted into Eq. (17) to cancel out the imaginary part of the normalised residual function. With the optimisation problem listed in Eqs. (18a) and (18b), the pseudo mode shape vectors of real numbers were thus obtained. By using the pseudo mode shape matrix, the equivalent mass, damping, and stiffness matrices of the solid foundation were estimated in Eqs. (14a)–(14c).

The results of the FRF curves both for the original and the equivalent solid foundations are plotted in Fig. 5. In this case, even by taking only the first four sets of modal parameters, the resulting FRF curves of the modified PMSM and the original PMSM were quite similar. However, these FRF curves began to deviate with those of the FE model at a frequency of 20 Hz, although all three of them were almost the same within the frequency range of 0–20 Hz. This could be attributed to the fact that the fifth natural frequency (30.856 Hz) was very close to the fourth natural frequency (27.848 Hz), and the deviation of the FRF curves was observed near the fourth natural frequency. To improve the accuracy of the results within the frequency range of 20–50 Hz, the identification procedures is expected to increase the number of modal parameters.

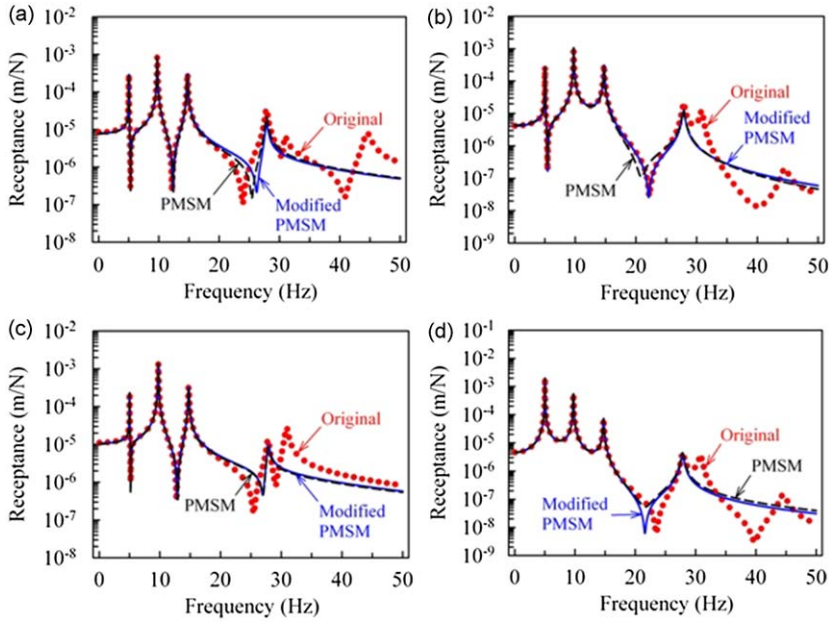

Fig. 5. Frequency-response function curves of the solid foundation taking the first four sets of modal parameters: (a) H_{22}, (b) H_{23}, (c) H_{33} and (d) H_{34}. ●, Original; ——, modified PMSM (equivalent); and – – –, PMSM (equivalent).

4.2. Equivalent solid foundation taking the first six sets of modal parameters and the weighting factors

To make the distribution of natural frequencies of the equivalent foundation within 0–50 Hz the same as those of the original, the first six sets of the modal parameters were taken into consideration. The dimension of the equivalent mass, damping, and stiffness matrices expanded from 4×4 to 6×6. Although the six sets of modal parameters were adopted, the actual existing number of components in the mode shape vector was four (i.e., two DOFs in each of the supports and a total of two supports on the system). Each mode shape vector (column vector) added the two assumed values at the fifth and sixth components as long as the formed mode shape vectors were linearly independent [20]. A prior check-up for the condition number of the pseudo mode shape matrix thus became necessary to ensure the non-singularity of the obtained matrix.

Fig. 6 shows the FRF curves of the original and equivalent solid foundations, respectively. The fifth and sixth natural frequencies have been included in the equivalent FRF curves. However, within the frequency range of 20–50 Hz, the equivalent FRF curves still did not fully match the original ones regardless of the PMSM or the modified PMSM. The notable deviation appeared in curves H_{23} and H_{34}. To further improve the accuracy of the FRF curves, the weighting factors $W_{22,4}$=100, $W_{23,4}$=100,$W_{34,4}$=500, $W_{34,5}$=500, and $W_{34,6}$=500 were introduced to the modified PMSM. These weighting factors as indicated in Eq. (18a) can be adjusted empirically by checking the obtained FRF results. For example, owing to larger deviations that appeared within the frequency range between 20–50 Hz, the weighting factors that corresponded to the residual functions of the fourth, fifth, and sixth modes were adjusted effectively after performing some trial procedures.

Fig. 7 depicts the resulting FRF curves for the original and equivalent solid foundations. As can be seen, the FRF curves of the modified PMSM with the weighting factors have the best fitting results. It should be noted that the deviations of the H_{23} and H_{34} curves shown in Fig. 6 have been corrected within the frequency range of 20–50 Hz. The calculated equivalent matrices for evaluating the FRF curves of the system with the equivalent solid foundation are listed in Table 2.

4.3. System with the equivalent solid foundation

The FRF curves of the original and the equivalent whole structures at the rotor journals are shown in Fig. 8. By applying the equivalent foundation matrices (Table 2) in the whole system, the fitting results of the FRF curves with the modified PMSM are shown to be much the same as the FE results within the frequency range of 0–30 Hz. Nevertheless, the curves of H_{23} and H_{34} between 30–45 Hz showed little deviations. This was because the seventh or higher modal parameters were not yet considered. This resulted in the not so satisfactory accuracy of the identified equivalent foundation matrices; whereas it was noted that with the equivalent matrices that came from the PMSM without modifications, obvious deviations were also observed after 25 Hz. In addition, larger errors in the (Equivalent-Original)/Original natural frequency ratios were distinguished at the sixth and seventh modes with 3.13% and 3.81%, respectively. In summary, with the dynamic properties of the system with the equivalent solid foundation fairly close to those of the system with the original

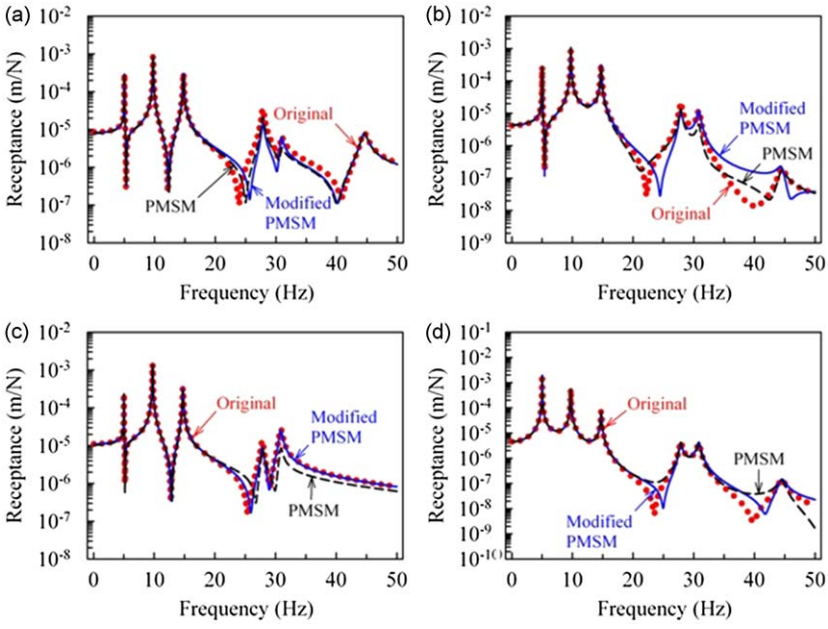

Fig. 6. Frequency-response function curves of the solid foundation taking the first six sets of modal parameters: (a) H_{22}, (b) H_{23}, (c) H_{33}, and (d) H_{34}. ●, Original; ——, modified PMSM (equivalent); and – – –, PMSM (equivalent).

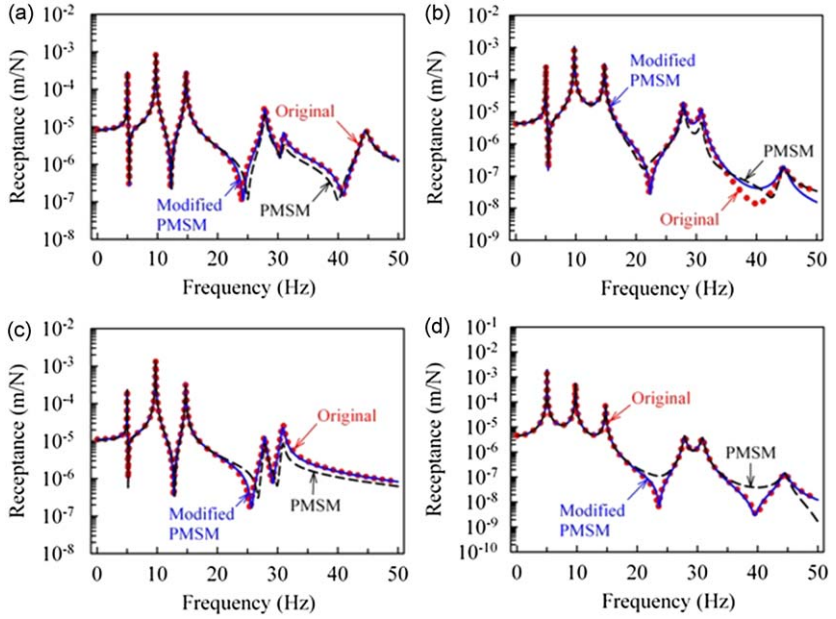

Fig. 7. Frequency-response function curves of the solid foundation taking the first six sets of modal parameters and the weighting factors: (a) H_{22}; (b) H_{23}; (c) H_{33}; (d) H_{34}. ●, Original; ——, modified PMSM (equivalent); – – –, PMSM (equivalent).

Table 2
Equivalent matrices (6×6) of the solid foundation.

Row	Column					
	1	2	3	4	5	6
Mass matrix						
1	26.652	120.021	6.922	−176.545	−52.807	7.483
2	120.021	1517.831	81.982	−2200.511	−643.132	88.992
3	6.922	81.982	19.415	−120.277	−34.987	4.818
4	−176.545	−2200.511	−120.277	3236.141	941.599	−130.281
5	−52.807	−643.132	−34.987	941.599	275.799	−38.251
6	7.483	88.992	4.818	−130.281	−38.251	5.318
Damping matrix						
1	57.149	192.642	−7.132	−293.461	−88.404	12.861
2	192.642	3311.861	137.661	−4456.441	−1300.731	177.048
3	−7.132	137.661	21.087	−184.168	−53.335	7.161
4	−293.461	−4456.441	−184.168	6057.331	1772.521	−242.687
5	−88.404	−1300.731	−53.335	1772.521	519.449	−71.316
6	12.861	177.048	7.161	−242.687	−71.316	9.850
Stiffness matrix						
1	71.463×10^4	2.414×10^6	-88.861×10^3	-3.676×10^6	-1.107×10^6	16.111×10^4
2	2.414×10^6	4.141×10^7	1.721×10^6	-5.573×10^7	-1.626×10^7	2.214×10^6
3	-88.861×10^3	1.721×10^6	26.355×10^4	-2.302×10^6	-66.679×10^4	89.546×10^3
4	-3.676×10^6	-5.573×10^7	-2.302×10^6	7.576×10^7	2.217×10^7	-3.035×10^6
5	-1.107×10^6	-1.626×10^7	-66.679×10^4	2.217×10^7	6.497×10^6	-89.215×10^4
6	16.111×10^4	2.214×10^6	89.546×10^3	-3.035×10^6	-89.215×10^4	12.323×10^4

solid foundation, it has been proven that the modified procedures in the PMSM are effective measures in improving the calculation accuracy.

5. Industrial application

In the previous case study with FE, the simulation results confirm without a doubt the feasibility of using the equivalent matrices to replace the original substructure in the dynamic analysis of the whole system. However, these results are all based on the numerical investigations. This section thus aims to apply the corresponding algorithm to practical industrial

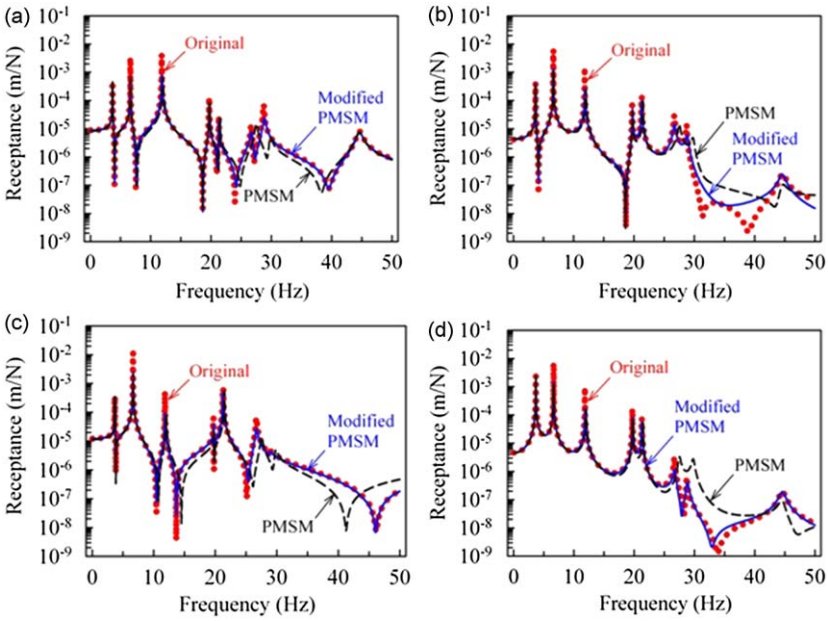

Fig. 8. Frequency-response function curves of the solid foundation system: (a) H_{22}, (b) H_{23}, (c) H_{33}, and (d) H_{34}. ●, Original; ——, modified PMSM (equivalent); and – – –, PMSM (equivalent).

applications. Toward this goal, the housing of an induction motor was adopted as a realistic case study to identify its equivalent matrices. Both sets of results obtained from using the presented method and the experimental investigations were discussed.

5.1. Squirrel-cage induction motor system

The squirrel-cage induction motor is one of the typical industrial rotating machineries currently being used. It is often seen in the manufacturing machinery to link to a hydraulic pump that serves as the power source in the hydraulic system of the machine. Fig. 9 shows the construction of the squirrel-cage motor system, which includes the main components such as the rotating shaft, ball bearings, and housing. As can be seen in the part of the rotor, the rotating shaft is mounted to the laminated silicon steel sheets and is supported by two ball bearings located near the front and rear ends of the shaft. On the part of the stator, the field copper coils are wound into a form of four poles with the laminated silicon steel sheets to receive the three-phase AC power of 100 Hz frequency. This, in turn, will produce a rotating magnetic field to drive the rotor up to a working speed of 3000 rpm. The bearing supports were specifically designed to be placed on the front and rear panels of the housing to simplify the assembly procedures.

In a previously published work [22], the authors developed a vibration analysis module for solving the dynamic behaviour of rotor–bearing systems by taking the motor as a studied case for demonstration. The housing assembly of the motor consists of its outer shell, the field copper coils built inside, and the laminated silicon steel sheets. Hence, the above-mentioned analysis has not yet considered the housing effect, because building an accurate model of housing is very difficult and time-consuming. Instead, the modified PMSM was adopted to estimate the equivalent matrices of the housing assembly without having to build the actual model as those in the traditional FE method.

5.2. Experimental setup

The schematic of the experimental setup for the tested housing is shown in Fig. 10. The motor housing is rigidly fixed through its bottom bracket with four bolts on a metal table with several mounting holes as shown in the figure. All of the rotor elements such as the rotating shaft, laminated silicon steel sheets, and bearings have been removed from the motor housing. Hence, the system of the housing structure merely consists of the laminated silicon steel sheets, field copper coils, panels, and bearing supports. The equivalent matrices can be estimated by performing modal testing at the bearing supports. The testing points were respectively denoted as 1-DOF and 2-DOF in the horizontal and vertical directions at the front support, as well as the 3-DOF and 4-DOF at the rear support. The accelerometer (KISTLER 8732A500) attached and the hammer (PCB 086C01) applied at these points, in turn, measure the signals of lateral acceleration and impulsive force with the sampling rate of 1.28 kHz. The corresponding FRF curves were calculated from the spectrum analyzer (SigLab Model 20-42) and were displayed on a laptop computer (IBM A30 2652) within the frequency range of 25–150 Hz to ensure the

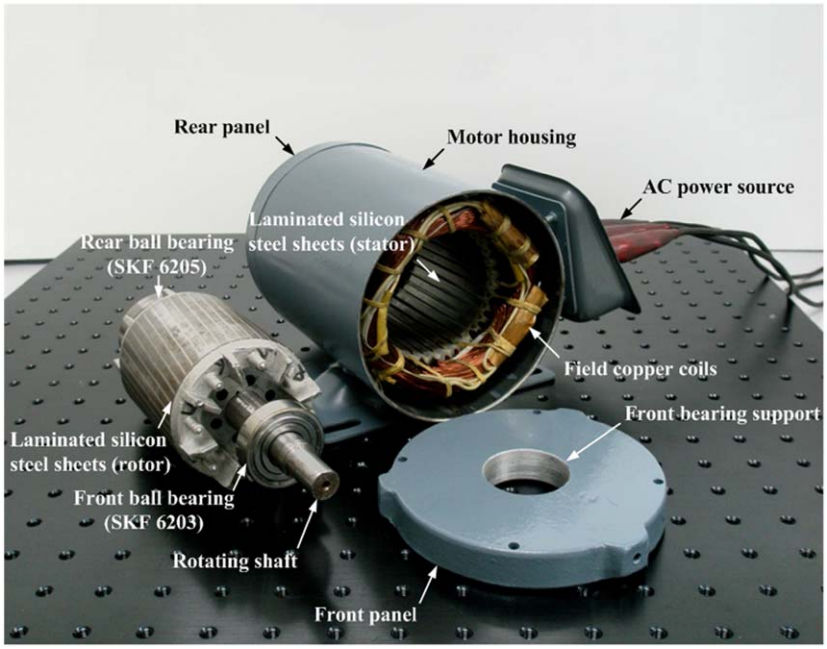

Fig. 9. Constructions of the squirrel-cage motor system.

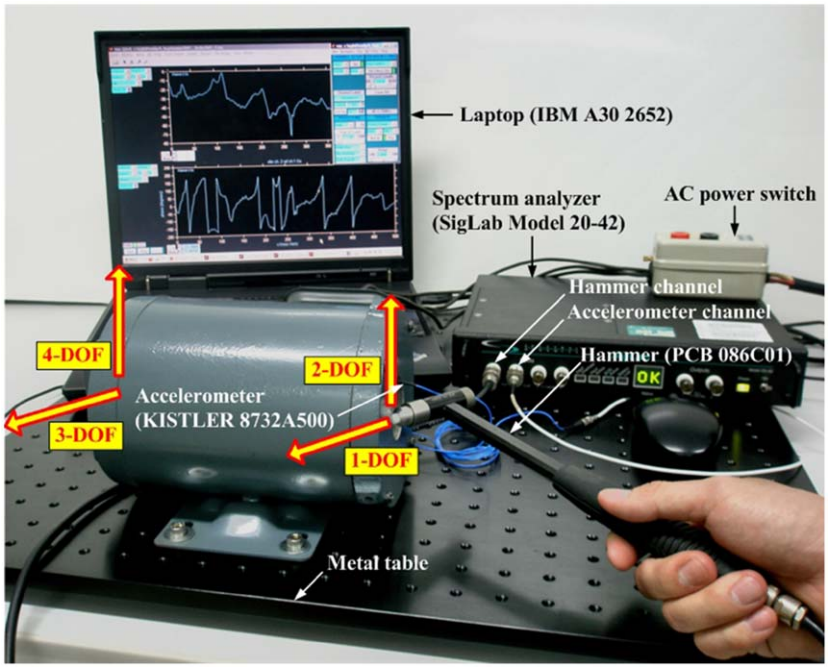

Fig. 10. Experimental setup for the modal testing of motor housing.

linear responses of sensor voltage. These FRF curves were used to construct the FRF matrix (Eq. (11)) once the initial identification procedure was initiated.

5.3. Equivalent motor housing

The FRF curves of the motor housing at the bearing supports were obtained from the experimental modal testing. The first four sets of modal parameters with their corresponding peak values were used to estimate the equivalent matrices

Table 3
Equivalent matrices (4×4) of the motor housing.

Row	Column			
	1	2	3	4
Mass matrix				
1	249.995×10^{-6}	87.365×10^{-6}	246.375×10^{-6}	-84.789×10^{-6}
2	87.365×10^{-6}	438.441×10^{-6}	338.806×10^{-6}	-309.701×10^{-6}
3	246.375×10^{-6}	338.806×10^{-6}	554.171×10^{-6}	-300.693×10^{-6}
4	-84.789×10^{-6}	-309.701×10^{-6}	-300.693×10^{-6}	265.361×10^{-6}
Damping matrix				
1	12.496×10^{-3}	8.822×10^{-3}	13.667×10^{-3}	-7.506×10^{-3}
2	8.822×10^{-3}	33.100×10^{-3}	26.711×10^{-3}	-23.648×10^{-3}
3	13.667×10^{-3}	26.711×10^{-3}	33.777×10^{-3}	-21.488×10^{-3}
4	-7.506×10^{-3}	-23.648×10^{-3}	-21.488×10^{-3}	18.985×10^{-3}
Stiffness matrix				
1	25.737	13.751	12.765	−13.016
2	13.751	110.327	107.081	−72.789
3	12.765	107.081	147.869	−87.827
4	−13.016	−72.789	−87.827	65.779

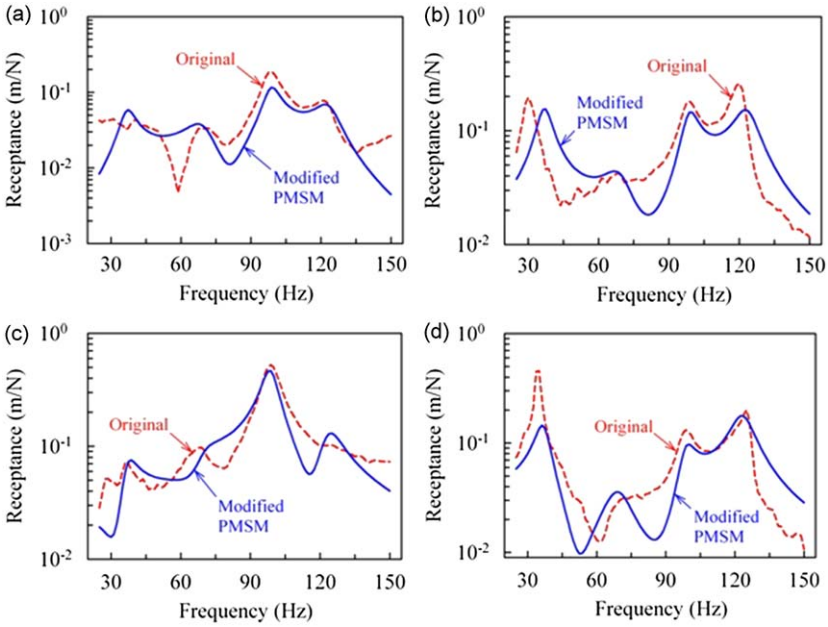

Fig. 11. Frequency-response function curves of the motor housing: (a) H_{12}, (b) H_{14}, (c) H_{24}, and (d) H_{34}. – – –, Original; ——, equivalent.

of the housing. The calculated equivalent matrices of the housing are listed in Table 3. The results of the FRF curves (H_{12}, H_{14}, H_{24}, and H_{34}) are plotted in Fig. 11. In the figure, the structure of the motor housing is hereby referred to as the *original motor housing,* while the estimated equivalent matrices of the solid foundation are referred to as the *equivalent motor housing*. The comparisons of the natural frequencies are listed in Table 4.

The figure shows that there is a deviation somewhere between the curves of the equivalent and the original, but their shapes are similar in nature. The ratios of the errors of frequency were within the range of $\pm 5\%$ except for the first natural frequency curve of H_{14}. The reasons behind the discrepancies between the results of identification and testing can be inferred from two aspects: the assumption of the theoretical model and the quality of the signal data.

In Eq. (8), the actual FRF was described as the sum of the numerous sets of modal parameters and mode shapes. The PMSM assumed that the effects of other modes for any peak values of FRF were ignored, and this simplified Eq. (8) into Eq. (10). The only set of modal parameters and peak value was adopted to evaluate the mode shape of the corresponding mode. On the other hand, each FRF curve needs to be reliable and highly correlated in order to obtain the correct modal parameters. The demand is usually associated with the properties of the sensors, the capability of the analyzer, and the correct testing manner.

Table 4
Natural frequency (Hz) comparisons of the original and equivalent motor housings.

Mode	Equivalent	Original			
		H_{12}	Error (%)	H_{14}	Error (%)
1	37.002	38.230	−3.212	30.993	19.388
2	69.454	68.585	1.267	69.542	−0.127
3	98.613	97.886	0.743	98.130	0.492
4	123.403	123.117	0.232	121.361	1.683
		Original			
		H_{24}	Error (%)	H_{34}	Error (%)
1	37.002	36.021	2.723	35.338	4.709
2	69.454	68.812	0.933	69.260	0.280
3	98.613	98.385	0.232	98.167	0.454
4	123.403	124.552	−0.923	125.557	−1.716

6. Conclusions

In this paper, the FRF curves at the bearing supports were utilised to establish the accurate equivalent mass, damping, and stiffness matrices of the foundation by using PMSM in tandem with the procedures of phase modification and numerical optimisation. Some of the significant conclusions are summarised as follows:

1. The numerical study showed that the equivalent mass, damping, and stiffness matrices of the foundation (substructure) can successfully replace the original substructure via the modified PMSM. Within a specific frequency range, the corresponding results for the dynamic properties of the rotor–bearing system equipped with the equivalent matrices of the foundation were the same as those of the system equipped with the FE model of foundation.
2. Increasing the number of sets of modal parameters led to the expansion of dimensions in the equivalent matrices' of dynamic properties at higher frequency ranges. The weighting factors of the objective function were adopted to enhance the weighting of the squares of the residual values at certain modes. Consequently, the deviation between the equivalent and original FRF curves can be corrected significantly at these modes.
3. To make the dynamic properties of the equivalent foundation match those of the N modes of the original foundation, at least $N+1$ sets of the modal parameters of the foundation FRF curves should be considered. In addition, to make the dynamic properties of the equivalent whole structure fit better with those of the N modes of the original whole structure, it was necessary to have at least $N+2$ sets of modal parameters of the foundation FRF curves.
4. The feasibility of the modified PMSM was confirmed experimentally via the study of a realistic motor housing. The results also showed that the dynamic properties of a complex substructure can be described as matrices with limited dimensions. The accuracy of the identified results depended on, among others, the number of modal participations, the precision of modal parameters, and the quality of measured FRF curve data.

The purpose of the modified PMSM described in this paper is to solve real-world engineering problems. Using the limited FRF data, engineers obtain the equivalent substructure model while avoiding tedious FE modelling processes. By associating the method with other applications, it can have a wide range of practical advantages, such as developing the online diagnostics of rotor system by improving its computer simulation efficiency.

Acknowledgments

The authors are deeply appreciative to the Taiwan Power Company for supporting this research.

References

[1] Y. Kang, Y.P. Chang, J.W. Tsai, L.H. Mu, Y.F. Chang, An investigation in stiffness effects on dynamics of rotor–bearing–foundation systems, *Journal of Sound and Vibration* 231 (2000) 343–374.
[2] R. Gasch, Vibration of large turbo-rotor in fluid-film bearing on an elastic foundation, *Journal of Sound and Vibration* 47 (1976) 53–73.
[3] J.C. Nicholas, J.K. Whalen, S.D. Franklin, Improving critical speed calculations using flexible bearing support FRF compliance data, *Proceedings of the 15th Turbomachinery Symposium,* College Station, TX, 1986, pp. 69–78.
[4] J.M. Vance, B.T. Murphy, H.A. Tripp, Critical speeds of turbomachinery: computer predictions vs. experimental measurements—part II: effect of tilt-pad bearings and foundation dynamics, *ASME Journal of Vibration, Acoustic, Stress, and Reliability in Design* 109 (1987) 8–14.
[5] R.W. Stephenson, K.E. Rouch, Generating matrices of the foundation structure of a rotor system from test data, *Journal of Sound and Vibration* 154 (1992) 467–484.

[6] P.F. Cavalcante, K.L. Cavalca, A method to analyze the interaction between rotor–foundation systems, *Proceedings of the International Modal Analysis Conference*, Santa Barbara, CA, 1998, pp. 775–781.
[7] M. Dias Jr., K.L. Cavalca, Experimental analysis of the dynamic behaviour of a turbomachine foundation structure, *Proceedings of the International Modal Analysis Conference*, Kissimmee, FL, 1999, pp. 966–972.
[8] K.L. Cavalca, P.F. Cavalcante, E.P. Okabe, An investigation on the influence of the supporting structure on the dynamics of the rotor system, *Mechanical Systems and Signal Processing* 19 (2005) 157–174.
[9] G. Diana, F. Cheli, A. Vania, A method to identify the foundation modal parameters through measurements of the rotor vibration, *4th International Conference on Vibrations in Rotating Machinery*, Edinburgh, Scotland, 1988, pp. 217–222.
[10] T.K. Tee, R. Stanway, J.E. Mottershead, A.W. Lees, Identification of turbomachinery foundations from run-down records—a preliminary experimental study, *4th International Conference on Vibrations in Rotating Machinery*, Edinburgh, Scotland, 1988, pp. 201–207.
[11] N.S. Feng, E.J. Hahn, Including foundation effects on the vibration behavior of rotating machinery, *Mechanical Systems and Signal Processing* 9 (1995) 243–256.
[12] M.G. Smart, M.I. Friswell, A.W. Lees, Estimating turbogenerator foundation parameters: model selection and regularization, *Proceedings of the Royal Society A: Mathematical, Physical and Engineering Sciences* 456 (2000) 1583–1607.
[13] A.W. Lees, M.I. Friswell, The evaluation of rotor imbalance in flexibly mounted machines, *Journal of Sound and Vibration* 208 (1997) 671–683.
[14] S. Edwards, A.W. Lees, M.I. Friswell, Experimental identification of excitation and support parameters of a flexible rotor–bearings–foundation system from a single run-down, *Journal of Sound and Vibration* 232 (2000) 963–992.
[15] J.K. Sinha, M.I. Friswell, A.W. Lees, The identification of the unbalance and the foundation model of a flexible rotating machine from a single run-down, *Mechanical Systems and Signal Processing* 16 (2002) 255–271.
[16] A.W. Lees, J.K. Sinha, M.I. Friswell, The identification of the unbalance of a flexible rotating machine from a single rundown, *ASME Journal of Engineering for Gas Turbines and Power* 126 (2004) 416–421.
[17] P. Pennacchi, N. Bachschmid, A. Vania, G.A. Zanetta, L. Gregori, Use of modal representation for the supporting structure in model-based fault identification of large rotating machinery: part 1—theoretical remarks, *Mechanical Systems and Signal Processing* 20 (2006) 662–681.
[18] P. Pennacchi, N. Bachschmid, A. Vania, G.A. Zanetta, L. Gregori, Use of modal representation for the supporting structure in model-based fault identification of large rotating machinery: part 2—application to a real machine, *Mechanical Systems and Signal Processing* 20 (2006) 682–701.
[19] R. Provasi, G.A. Zanetta, A. Vania, The extended Kalman filter in the frequency domain for the identification of mechanical structures excited by sinusoidal multiple inputs, *Mechanical Systems and Signal Processing* 14 (2000) 327–341.
[20] T. Yang, M.C. Chen, K.L. Koai, Dynamic modeling of structures using pseudo mode shape method, *III European Conference on Computational Mechanics: Solids, Structures and Coupled Problems in Engineering*, Lisbon, Portugal, 2006, pp. 5–9.
[21] T. Yang, M.C. Chen, K.L. Koai, Modeling of the foundations of rotor–bearing systems by pseudo mode shape method, *Monthly Journal of Taipower's Engineering* 697 (2006) 1–9.
[22] Y.S. Chen, Y.D. Cheng, J.J. Liao, C.C. Chiou, Development of a finite element solution module for the analysis of the dynamic behavior and balancing effects of an induction motor system, *Finite Elements in Analysis and Design* 44 (2008) 483–492.
[23] D.J. Ewins, *Modal Testing: Theory and Practice*, Research Studies Press Ltd., London, 1984.
[24] J. Nocedal, S.J. Wright, *Numerical Optimization*, Springer, New York, 2006.
[25] H.D. Nelson, J.M. McVaugh, The dynamics of rotor-bearing systems using finite elements, *ASME Journal of Engineering Industry* 98 (1976) 593–600.
[26] H.D. Nelson, Finite rotating shaft element using Timoshenko beam theory, *ASME Journal of Mechanical Design* 102 (1980) 793–803.
[27] N. Bachschmid, P. Pennacchi, A. Vania, Identification of multiple faults in rotor systems, *Journal of Sound and Vibration* 254 (2002) 327–366.